

# A fast and robust computational method for the ionization cross sections of the driven Schrödinger equation using an $\mathcal{O}(N)$ multigrid-based scheme

S. Cools<sup>a</sup>, W. Vanroose<sup>a</sup>

<sup>a</sup>*Applied Mathematics Research Group, Department of Mathematics and Computer Science, University of Antwerp, Middelheimlaan 1, 2020 Antwerp, Belgium*

---

## Abstract

This paper extends the complex contour approach for far field map computation [S. Cools, B. Reys, W. Vanroose, An Efficient Multigrid Calculation of the Far Field Map for Helmholtz and Schrödinger Equations, SIAM J. Sci. Comp. 36(3) B367–B395 (2014)] that allows for a highly efficient multigrid-based calculation of the far field map for Helmholtz and Schrödinger type scattering problems. In this work we propose to add an advanced Coupled Channel Correction Step (CCCS) after each multigrid (MG) V-cycle, which accounts for the presence of localized bound states in the solution. The combined iterative solution scheme (MG-CCCS) is shown to feature significantly improved convergence rates over the classical MG method at energies where bound states dominate the solution, resulting in a fast and scalable solution method to the Schrödinger break-up problem for any energy regime. We show that this ultimately leads to an overall robust method for the computation of the ionization cross sections for electron-impact models. The proposed MG-CCCS method is validated on a 2D Temkin-Poet model problem, and convergence results using the MG-CCCS scheme both as a solver and preconditioner are provided to support the  $\mathcal{O}(N)$  scalability of the method.

---

## 1. Introduction

Over the past decades significant work has been performed on the computational simulation of electron-impact scattering. The cross sections of 2D and 3D electron-impact ionization problems were calculated by McCurdy et al. in [19, 22, 1], and more recently [18, 28]. However, the classical algorithms for the computation of the ionization cross sections for a general Schrödinger type scattering problem are notably very demanding in terms of computational resources, often requiring supercomputing infrastructure. This computational overhead primarily originates from the computation of the high-dimensional scattering solutions governed by Schrödinger's equation, which are notoriously hard to obtain using either classical direct methods or iterative solvers. Hence, numerical simulations of the far field behaviour for molecular break-up problems is generally computationally challenging. The intent of this work is to design an efficient and scalable method for the computation of the cross sections of the  $d$ -dimensional driven Schrödinger equation. Moreover, we aim at computing the single differential cross section (SDCS) and total cross section (TCS) for Schrödinger type scattering problems using a multigrid-based method which only scales linearly in the number of unknowns.

Multigrid [5] is an efficient iterative solution method for the large and sparse linear systems that appear in the numerical solution of Laplace-type partial differential equations (PDEs). The method relies upon a hierarchy of discretizations of the problem to accelerate convergence to the solution of the problem at the finest discretization level. The key functional concept of the multigrid method is the synergy between the so-called smoother, i.e. a basic iterative update step such as weighted Jacobi or Gauss-Seidel which is applied at each level, and a coarse grid correction scheme that solves the error equation on a coarser

---

*Email addresses:* [siegfried.cools@uantwerpen.be](mailto:siegfried.cools@uantwerpen.be) (S. Cools), [wim.vanroose@uantwerpen.be](mailto:wim.vanroose@uantwerpen.be) (W. Vanroose)

discretization level and consequently uses the interpolated error to correct the fine-level guess to the solution [5, 6]. From the spectral analysis point of view, the smoother basically removes the oscillatory parts from the error, resulting in a remaining error which is smooth enough to be represented at the coarser levels of the discretization hierarchy. Applying this recursively typically leads to an  $\mathcal{O}(N)$  scheme for the solution of Laplace-type PDEs, where  $N$  is the number of unknowns at the finest level. The multigrid method is therefore commonly used to solve high-dimensional Poisson problems, where it is particularly efficient due to its scalability. However, multigrid-preconditioned Krylov methods have also successfully been applied as solvers for e.g. fluid flow models, see [11]. Indeed, multigrid is in practice often used as a preconditioner to accelerate the convergence of Krylov subspace iterations such as CG or GMRES [27]. It has been shown in the literature that the use of multigrid as a Krylov method preconditioner results in an efficient and scalable solution method for Laplace-type problems, featuring a convergence rate which is independent of the number of unknowns [26].

Although multigrid is customarily applied as both a solver and preconditioner for a wide range of Laplace-type PDEs, it is well-known that the classical multigrid method (like any iterative solver) utterly breaks down when applied to Helmholtz or Schrödinger problems. The reason for this convergence failure is best understood by analyzing the spectral properties of the corresponding operator. Due to the intrinsic indefiniteness of the discretized Helmholtz operator, the occurrence of near-zero coarse level eigenvalues destroys the stability of both smoother and two-grid correction scheme, leading to a possibly highly instable multigrid scheme [12, 14]. In the past decades much effort has been performed to overcome the stability issues of multigrid for Helmholtz equations. Most notably, it has been proposed by Erlangga et al. in [13] that multigrid can be successfully used as a solver for the complex shifted (i.e. damped) Helmholtz equation. This perturbed problem is known as Complex Shifted Laplacian (CSL), and is nowadays commonly used as a preconditioner for Helmholtz problems [4]. Alternatively, the underlying numerical grid can be rotated into the complex domain to yield an equivalent damped Helmholtz problem, which is known as Complex Stretched Grid (CSG) [21]. This technique shows significant resemblances to Exterior Complex Scaling (ECS) [25].

In this paper the functionality of the multigrid method on damped Helmholtz and Schrödinger equations is exploited to effectively construct an efficient computational method for the far field map (ionization cross sections) of Schrödinger type scattering problems. The computation of the far field map can typically be seen as a two-step process: the first step consists of solving the underlying driven Schrödinger equation on a bounded numerical box, whereas in the second step an integral over the scattering solution on this domain has to be calculated [17, 8]. The main computational bottleneck generally lies within the first step, since this requires the efficient solution of the Schrödinger-type scattering equation, which is typically hard to obtain using classical iterative methods. However, in [9] it was proposed that the classical far field integral over the real-valued  $d$ -dimensional bounded domain can alternatively be replaced by an integral over a complex manifold. Furthermore, it was shown that this complex contour technique yields an identical far field map. Moreover, the first step in the calculation now consists of solving a damped Helmholtz or Schrödinger equation, which can be very efficiently achieved using e.g. multigrid. In this way the main computational bottleneck in the far field map computation is overcome, since the numerical solution on the bounded box can effectively be solved using a scalable iterative method.

In this work we use the complex contour approach introduced in [9] to compute the ionization cross sections of 2D Schrödinger type scattering problems. The multigrid method used for the solution of the complex-valued driven Schrödinger problem (step 1) is further extended by the addition of a so-called Coupled Channel Correction Scheme (CCCS), which ensures the efficiency of the proposed solver for all possible energy levels by specifically eliminating the bound states, i.e. low-dimensional localized waves travelling along the domain edges. The Coupled Channel Correction Scheme is derived analytically, and we expound on its numerical properties through an eigenvalue analysis. Numerical results in 2D are provided to illustrate that the combination of multigrid and the Coupled Channel correction (MG-CCCS) effectively leads to a

fast, scalable and robust iterative scheme for solving the driven Schrödinger equation for any energy regime.

We additionally comment on the choice of the complex rotation angle in this work. Although from the analytical point of view there are no fundamental restrictions on the magnitude of the complex rotation, and the multigrid solver clearly benefits from a heavy damping of the problem, we show that choosing the rotation angle too large may result in numerical instabilities when calculating the integral in the second step of the computation. Indeed, the choice of the rotation angle is shown to be restricted by the numerical implementation, and is thus in practice a trade-off between multigrid performance for computing the scattered wave solution (step 1) and computational stability of the far field integral (step 2).

The Temkin-Poet (TP) model will be used throughout this work as an approximation to an impact ionization problem, where only s-waves are used to describe the scattered electrons. This model has a long history as a standard benchmark problem for general Schrödinger scattering problems, see e.g. [22], where a two-dimensional TP model was used to describe the impact ionization of molecular hydrogen. Similarly, the impact ionization of helium can be modelled by a 3D Temkin-Poet model [28]. Hence, the semi-realistic TP model problem serves as the primary test case for numerical validation of the proposed MG-CCCS method in this paper.

The outline of the article is the following. In Section 2 we introduce the notation and basic concepts that will be used throughout this work. Additionally, we briefly revisit the complex contour method for the computation of the far field map, which was initially proposed in [9], and we comment on the related spectral properties of the complex rotated Schrödinger equation. This discussion motivates the need for the so-called Coupled Channel Correction Scheme (CCCS) introduced in Section 3, which is used to compensate for the deterioration of multigrid convergence in certain energy regimes where bound states dominate the solution. In Section 4 we comment on the implementation of the Coupled Channel scheme and the influence of the complex rotation angle on numerical accuracy. Taking into account these remarks, the single differential and total cross sections of a 2D Temkin-Poet model problem are computed using the MG-CCCS method. We illustrate the efficiency of the combined MG-CCCS method both as a solver and a preconditioner in Section 5, and demonstrate the robustness of the MG-CCCS preconditioned Krylov solvers with respect to the energy of the system. Section 6 concludes this work alongside a discussion on the topic.

## 2. The Schrödinger equation and the far field map

The  $d$ -dimensional time-independent driven Schrödinger equation for a system with unit mass is given by

$$\left(-\frac{1}{2}\Delta + V(\mathbf{x}) - E\right)u(\mathbf{x}) = f(\mathbf{x}), \quad \text{for } \mathbf{x} \in \mathbb{R}^d, \quad (1)$$

where  $\Delta$  is the  $d$ -dimensional Laplacian,  $V(\mathbf{x})$  is a scalar potential,  $E$  is the energy of the system,  $u$  is the outgoing wave function and  $f$  is the right-hand side, representing the effect of an incoming wave or the influence of an optical perturbation such as interaction with light. The operator  $H = -\frac{1}{2}\Delta + V(\mathbf{x})$  is the Hamiltonian. This type of problem typically originates from the expansion of a 6D or 9D scattering problem in spherical harmonics, see [1, 28], in which each particle is expressed in terms of its spherical coordinates, resulting in a coupled system of 2D (or 3D) equations. The potentials then include angular potentials like  $l(l+1)/r^2$  related to the partial wave angular momentum. Note that the differential operators only appear on the diagonal blocks of such a coupled system.

### 2.1. The 2D and 3D Schrödinger equation: notation and basic properties

For the 6D scattering problem, these diagonal blocks take the form of a two-dimensional Schrödinger equation

$$\left(-\frac{1}{2}\Delta + V_1(x) + V_2(y) + V_{12}(x, y) - E\right)u(x, y) = f(x, y), \quad x, y \geq 0, \quad (2)$$

with boundary conditions

$$\begin{cases} u(x, 0) = 0 & \text{for } x \geq 0 \\ u(0, y) = 0 & \text{for } y \geq 0 \\ \text{outgoing} & \text{for } x \rightarrow \infty \text{ or } y \rightarrow \infty, \end{cases} \quad (3)$$

where  $V_1(x)$  and  $V_2(y)$  are the one-body potentials that can include angular potentials like  $l(l+1)/r^2$  where  $l = 0, 1, 2, \dots$  depending on the angular momentum,  $V_{12}(x, y)$  is a two-body potential and  $E$  is the total energy of the system. Since the arguments  $x$  and  $y$  are in fact radial coordinates in the partial wave expansion, homogeneous Dirichlet boundary conditions are implied at the  $x = 0$  and  $y = 0$  boundaries. The potentials  $V_1$ ,  $V_2$  and  $V_{12}$  are generally analytical functions that decay as the radial coordinates  $x$  and  $y$  become large. In the case of the 9D scattering problem, the model problem derived through a partial wave expansion gives rise to a 3D Schrödinger problem

$$\begin{aligned} & \left( -\frac{1}{2}\Delta + V_1(x) + V_2(y) + V_3(z) \right. \\ & \left. + V_{12}(x, y) + V_{23}(y, z) + V_{13}(z, x) - E \right) u(x, y, z) = f(x, y, z), \quad x, y, z \geq 0, \end{aligned} \quad (4)$$

with boundary conditions

$$\begin{cases} u(x, y, 0) = 0 & \text{for } x, y \geq 0 \\ u(0, y, z) = 0 & \text{for } y, z \geq 0 \\ u(x, 0, z) = 0 & \text{for } x, z \geq 0 \\ \text{outgoing} & \text{for } x \rightarrow \infty \text{ or } y \rightarrow \infty \text{ or } z \rightarrow \infty, \end{cases} \quad (5)$$

In the context of the simulation of electron impact ionization, at least two electrons need to be described: the electron particle in the target and the impinging electron. This leads to a 6D Schrödinger equation, 3D for each particle. The potential is then typically split into a sum of one-body potentials and a two-body potential. Here the one-body potentials model the attraction of each electron by the nuclear charge, whereas the two-body potential simulates the electron-electron repulsion. More generally, for  $p$  particles, the potential  $V(\mathbf{x})$  with  $\mathbf{x} = (\mathbf{x}_1, \dots, \mathbf{x}_p)$  can be written as

$$V(\mathbf{x}) = \sum_{i=1}^p V_i(\mathbf{x}_i) + \sum_{i<j}^p V_{ij}(\mathbf{x}_i, \mathbf{x}_j) = \bar{V}_1(\mathbf{x}) + \bar{V}_2(\mathbf{x}). \quad (6)$$

For notational convenience, we use  $\bar{V}_1$  to denote the sum of all one body potentials and  $\bar{V}_2$  for the sum of the two-body potentials throughout the following sections.

## 2.2. Link with the $d$ -dimensional Helmholtz equation

Depending on the total energy of the system,  $E \in \mathbb{R}$ , the above Schrödinger system allows for scattering solutions, in which case equation (1) can be reformulated as a Helmholtz equation of the form

$$(-\Delta - k^2(\mathbf{x})) u(\mathbf{x}) = g(\mathbf{x}), \quad \text{for } \mathbf{x} \in \mathbb{R}^d, \quad (7)$$

where the spatially dependent wavenumber  $k(\mathbf{x})$  is defined by  $k^2(\mathbf{x}) = 2(E - V(\mathbf{x}))$  and the right-hand side is  $g(\mathbf{x}) = 2f(\mathbf{x})$ . The experimental observations from this type of quantum mechanical systems are typically far field maps of the solution [28]. In many quantum mechanical systems the potential  $V(\mathbf{x})$  is an analytical function, which suggests analyticity of the spatially-dependent wavenumber  $k(\mathbf{x})$  in the above Helmholtz equation. Additionally, the potential  $V(\mathbf{x})$ , and hence the wavenumber  $k(\mathbf{x})$ , is often decaying in function of growing  $\mathbf{x}$ . These observations prove particularly valuable in the context of this paper.

### 2.3. The single, double and triple ionization regimes

We now briefly expound on the physical interpretation of the 3D Schrödinger system in which  $V_1$ ,  $V_2$  and  $V_3$  are assumed to be identical one-body potentials and  $V_{12}$ ,  $V_{23}$  and  $V_{31}$  are, similarly, assumed to be identical two-body potentials. The 2D case is also covered here by means of a simple restriction. Depending on the strength of the one-body potentials  $V_1$ ,  $V_2$  and  $V_3$ , the problem allows for so-called single ionization waves, which are localized evanescent waves that propagate along the edges of the domain. If the attraction of  $V_1$  is strong enough, there exists a one-dimensional eigenstate  $\phi_n(x)$  with a negative eigenvalue  $\lambda_n < 0$ , characterized by the one-dimensional Helmholtz equation

$$\left( -\frac{1}{2} \frac{d^2}{dx^2} + V_1(x) \right) \phi_n(x) = \lambda_n \phi_n(x), \quad \text{for } x \geq 0. \quad (8)$$

Note that  $\phi_n(0) = 0$  and  $\phi_n(x \rightarrow \infty) = 0$ . If the two-body potential  $V_{12}(x, y)$  is negligibly small, then there automatically exists a bound state of the 2D subsystem, since each state  $\phi_n(x)\phi_n(y)$  is an eigenstate of the separable Hamiltonian  $(-1/2)\Delta + V_1(x) + V_2(y)$  with eigenvalue  $2\lambda_n$ . In the presence of a small but non-negligible two-body potential, this state will be slightly perturbed, resulting in an eigenstate  $\phi_n(x, y)$  with eigenvalue  $\mu_n$  that fits the 2D subsystem

$$\left( -\frac{1}{2}\Delta + V_1(x) + V_2(y) + V_{12}(x, y) \right) \phi_n(x, y) = \mu_n \phi_n(x, y), \quad x, y \geq 0. \quad (9)$$

The corresponding eigenvalue is  $\mu_n \approx 2\lambda_n < \lambda_n < 0$ . This ordering is typical for realistic atomic and molecular systems [2]. Similarly, the 3D system will have an eigenstate that looks approximately like  $\phi_n(x, y)\phi_n(z)$ , or any of its coordinate permutations. The fully 3D eigenstate  $\phi_n(x, y, z)$  fits the equation

$$\left( -\frac{1}{2}\Delta + V_1(x) + V_2(y) + V_3(z) + V_{12}(x, y) + V_{23}(y, z) + V_{13}(z, x) \right) \phi_n(x, y, z) = \nu_n \phi_n(x, y, z), \quad x, y, z \geq 0, \quad (10)$$

where  $\nu_n \approx \mu_n + \lambda_n \approx 3\lambda_n$ . Assuming that the potentials are such that  $\nu_n < \mu_n < \lambda_n < 0$ , there are four possible regimes of interest in equation (4), depending on the total energy  $E$ . First, for  $E < \nu_n$ , the problem is easy to solve numerically, but no interesting physical reactions occur in this regime. Similarly, for  $\nu_n < E < \mu_n$ , there are no scattering states in the solution. For energy levels  $\mu_n < E < \lambda_n$ , single ionization scattering occurs, i.e. there exist scattering solutions that are localized along one of the three axes in the 3D domain. These solutions take the form  $v(z)\phi_n(x, y)$  as  $z \rightarrow \infty$ , where  $\phi_n(x, y)$  is the eigenstate of (9) and  $v(z)$  is a scattering solution satisfying outgoing wave boundary conditions (and similarly for the respective coordinate permutations). For energies  $\lambda_n < E < 0$ , both single and double ionization occur simultaneously. The solution contains – besides single ionization waves – double ionization waves of the form  $w(y, z)\phi_n(x)$ , where  $\phi_n(x)$  is an eigenstate of (8) and  $w(y, z)$  is a 2D scattering state satisfying the outgoing wave boundary conditions. These waves are localized along the faces of the 3D domain, where one of the three coordinates is small. Finally, for  $E > 0$ , the solution contains, in addition, triple ionization waves. These are waves that describe a quantum mechanical system that is fully broken up into its sub-particles. In this case, all three relative coordinates  $x$ ,  $y$  and  $z$  can become large, resulting in a wave that extends to the entire domain.

### 2.4. The far field map: computation of the ionization cross sections

In physical experiments differential cross sections are measured for the fragments that emerge from the break-up problem. These cross sections are probability distributions describing the probability of the particle emerging in a certain direction after the breakup. Since in practical applications the distance from the target to the detector is typically much larger than the size of the system, the measured cross sections are in fact far field maps of the scattered wave solution.

The numerical calculation of the far field map is a two-step process. First, the Schrödinger equation (1) is discretized, meaning the solution is represented on a finite numerical grid and the differential operators are represented by algebraic matrix operators. In this work, we generally use an equidistant, dimension-uniform discretization where the number of grid points per spatial dimension is denoted by  $N$  (unless explicitly stated otherwise). The infinite domain  $\mathbb{R}^d$  is replaced by a finite domain using absorbing boundary conditions or absorbing layers, implemented using e.g. Perfectly Matched Layers (PML) [3] or Exterior Complex Scaling (ECS) [18]. This results in a large linear system of the form

$$\sum_{j=1}^N \left( -\frac{1}{2} \Delta_{ij}^h + V_{ij} - E \delta_{ij} \right) u_i^N = f_i, \quad i = 1, \dots, N, \quad (11)$$

where  $\Delta_{ij}^h$  is the discrete representation of the Laplacian which is sparse and typically depends on a discretization parameter  $h$ ,  $V_{ij}$  is the representation of the potential, which is often diagonal, and  $u_i$  and  $f_i$  are respectively the solution and the right-hand side, represented on the grid. The construction of  $\Delta^h$  in the presence of an absorbing boundary layer is discussed in [1]. In the first step of the classical far field map calculation the linear system (11) is then solved resulting in  $u^N$ . Due to the incorporation of absorbing boundary conditions the system may no longer be Hermitian, but rather complex symmetric. The spectral properties of the operator  $\Delta^h$  for a finite difference discretization with an ECS absorbing layer are discussed in Reps et al. [21]. Similar to the Helmholtz equation, the resulting system is indefinite and is hence very hard to solve using iterative methods such as multigrid preconditioned Krylov subspace methods, the traditional method of choice for large and sparse linear systems [14]. In 2006, the so-called complex shifted Laplacian (CSL) preconditioner was presented by Erlangga et al. [13], which allows for a more efficient solution to the above indefinite problem. However, perfect Krylov scalability in function of the wavenumber (or energy) is generally hard to achieve.

The second step in the calculation extracts the far field map from the numerical scattered wave solution  $u^N$  to Eqn. (11). Indeed, solving equation (11) yields the numerical solution inside a bounded discretization box. However, what is measured in practice is the probability distribution far away from the object. An additional post-processing step is hence required to translate the numerical solution into the far field map. We explain the extraction of the far-field map on the continuous equation. Splitting the potential  $V$  in one-body and two-body operators, see (6), allows us to rewrite the Schrödinger equation (1) as

$$\left( -\frac{1}{2} \Delta + \bar{V}_1(\mathbf{x}) - E \right) u(\mathbf{x}) = f(\mathbf{x}) - \bar{V}_2(\mathbf{x})u(\mathbf{x}), \quad \forall \mathbf{x} \in \mathbb{R}^d.$$

For separable potentials such as the one-body potentials, an explicit analytical expression exists which satisfies

$$\left( -\frac{1}{2} \Delta + \bar{V}_1(\mathbf{x}) - E \right) G(\mathbf{x}, \mathbf{y}) = \delta(\mathbf{x} - \mathbf{y}). \quad (12)$$

This fundamental solution  $G(\mathbf{x}, \mathbf{y})$  is called the Green's function, and it allows to write the solution  $u$  as

$$u(\mathbf{x}) = \int_{\mathbb{R}^d} G(\mathbf{x}, \mathbf{y}) (f(\mathbf{y}) - \bar{V}_2(\mathbf{y})u(\mathbf{y})) d\mathbf{y}. \quad (13)$$

Note that this integral can effectively be calculated by substituting the numerical solution  $u^N$  to the linear system (11) obtained in the first step into the integrand. This approach has been successfully used to solve challenging break up problems [8, 17, 18]. In this work we assume that the source term  $f(\mathbf{y})$  is compactly supported (or exponentially decaying) and, moreover, that the two-body potentials  $\bar{V}_2(\mathbf{y})$  are exponentially decaying, which are natural assumptions in the context of impact ionization problems. Hence, since  $f(\mathbf{y})$  and  $\bar{V}_2(\mathbf{y})$  are zero outside the numerical domain, the integral is replaced by a finite integral over the numerical domain that is used in the first step.

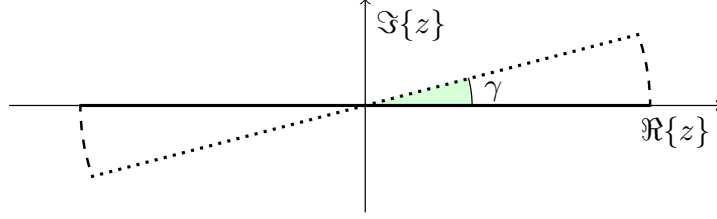


Figure 1: Schematic representation of the complex contour for the far field integral calculation illustrated in 1D. The full line represents the real domain  $\Omega$ , the dotted and dashed lines represent the subareas  $Z_1 = \{\mathbf{x}e^{i\gamma} : x \in \Omega \subset \mathbb{R}\}$  and  $Z_2 = \{be^{i\theta} : b \in \partial\Omega, \theta \in [0, \gamma]\}$  of the complex contour respectively.

In practice, the far field maps of (9) are thus Green's integrals over the solution, see [18]. Indeed, for a 2D problem setting where  $\mathbf{x} = (x, y)$ , the single ionization amplitude  $s_n(E)$ , which represents the total number of single ionized particles, is given by

$$s_n(E) = \int_{\Omega} \phi_{k_n}(x)\phi_n(y) [f(x, y) - V_{12}(x, y)u(x, y)] dx dy, \quad (14)$$

where  $k_n = \sqrt{2(E - \lambda_n)}$ . Here the function  $\phi_n$  is a one-body eigenstate, i.e. a solution of equation (8) with corresponding eigenvalue  $\lambda_n$ , and the function  $\phi_{k_n}$  is a regular, normalized solution of the homogeneous Helmholtz equation

$$\left(-\frac{1}{2} \frac{d^2}{dx^2} + V_1(x) - \frac{1}{2}k^2\right) \phi_k = 0, \quad (15)$$

where  $k = k_n$  and  $\phi_{k_n}$  is normalized by  $1/\sqrt{k_n}$ . Similarly, the double ionization cross section  $\zeta(k_1, k_2)$ , which measures the total number of double ionized particles, is defined by the integral

$$\zeta(k_1, k_2) = \int_{\Omega} \phi_{k_1}(x)\phi_{k_2}(y) (f(x, y) - V_{12}(x, y)u(x, y)) dx dy, \quad x, y \geq 0, \quad (16)$$

where both  $\phi_{k_1}(x)$  and  $\phi_{k_2}(y)$  are solutions to (15), with  $k_1 = \sqrt{2E} \sin(\alpha)$  and  $k_2 = \sqrt{2E} \cos(\alpha)$ , respectively, and  $\alpha \in [0, \pi/2]$  such that  $k_1^2 + k_2^2 = 2E$ . The total double ionization cross section is defined as the integral

$$\sigma_{tot}(E) = \int_0^E \sigma(\sqrt{2\epsilon}, \sqrt{2(E - \epsilon)}) d\epsilon, \quad (17)$$

where

$$\sigma(k_1, k_2) = \frac{8\pi^2}{k_0^2} \frac{1}{k_1 k_2} |\zeta(k_1, k_2)|^2. \quad (18)$$

### 2.5. Deforming the far field integral: the complex contour approach

The traditional far field map calculation is generally not scalable to very large, high-dimensional multiparticle problems. The main computational bottleneck lies in solving the linear system (11). This system has similar properties to the indefinite Helmholtz problem that appears in e.g. seismic inversion [23]. The construction of efficient solvers for the indefinite Helmholtz system is still an open and active research topic within the applied mathematics community.

However, since we are in fact not interested in the numerical solution  $u^N$  to (11) itself, but rather in the far field map of this solution, i.e. a Green's integral over  $u^N$ , the actual path of integration can be deformed as an additional degree of freedom. Indeed, it was suggested in [9] that the integral in equation (13) can alternatively be evaluated along a complex contour  $Z \subset \mathbb{C}^d$ , i.e.

$$u(\mathbf{x}) = \int_Z G(\mathbf{x}, \mathbf{y}) (f(\mathbf{y}) - \bar{V}_2(\mathbf{y})u(\mathbf{y})) d\mathbf{y}. \quad (19)$$

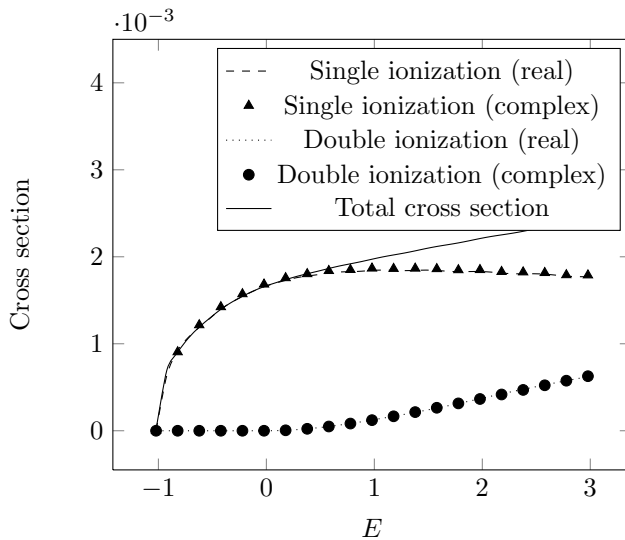


Figure 2: Comparison of the single and double ionization total cross sections calculated using the numerical scattered wave solution  $u^N$  to (2). Computation performed on (a) a traditional real-valued ECS grid with  $\theta = 25.7^\circ$  and (b) a full complex contour with  $\gamma = 8.5^\circ$ . The energy range starts at the single ionization threshold  $E = -1$ , corresponding to a strictly positive cross section. Double ionization occurs for energy levels  $E > 0$ .

rather than the physical real-valued domain  $\Omega \subset \mathbb{R}^d$ . The complex valued domain  $Z$  is illustrated schematically for the 1D case in Figure 1. The illustrated complex contour grid can be readily extended to  $d$  dimensions through the use of Kronecker products. Note that the integral over the subdomain  $Z_2$  vanishes; hence, the integral (19) is in fact only evaluated along the complex rotated grid  $Z_1 = \{\mathbf{x}e^{i\gamma} : \mathbf{x} \in \Omega \subset \mathbb{R}^d\}$ .

The far field map computation from the complex formulation (19) now requires the Schrödinger equation to be solved along a complex valued contour in order to obtain  $u(\mathbf{y})$  for all  $\mathbf{y} \in Z$ . However, it was shown in the literature [13, 21] that the spectral properties of the corresponding Schrödinger operator discretized along the complex contour are favorable for iterative solution. Indeed, equation (1) is reduced to a damped equation along the contour, which is much more amenable to iterative solution, particularly using multigrid. A key requirement for the validity of the complex contour integral reformulation (19) is the observation that the potentials appearing in the context of quantum mechanical break-up problems are continuous functions everywhere in the domain except at the exact nuclear positions. This is in contrast to many engineering and seismic problems, where the potential (or wavenumber) often represents objects that exhibit material jumps.

We briefly recap some of the key results from our previous work in [9], where the applicability of the complex contour method on 2D and 3D Schrödinger equations describing a quantum mechanical scattering problem was validated. Figure 2 shows the rate of single and double ionization as a function of the total energy  $E$  for a 2D electron-impact ionization Schrödinger-type model problem of the form (2) with right-hand side source term  $f(x, y) = \exp(-3(x + y)^2)$ . The potentials in this model problem are exponential functions defined as  $V_1(x) = -4.5 \exp(-x^2)$ ,  $V_2(y) = -4.5 \exp(-y^2)$  and  $V_{12}(x, y) = 2 \exp(-(x + y)^2)$ . The dashed and dotted lines on Figure 2 represent the single and double ionization amplitudes calculated using the traditional real-valued method with ECS absorbing boundary conditions [18]. The corresponding 2D scattering problems (2) are solved on a numerical domain  $\Omega = [0, 15]^2$  covered by a finite difference grid consisting of 300 grid points in every spatial dimension. Additionally, an ECS absorbing boundary layer starts at  $x = 15$  and  $y = 15$ , respectively, and implements the outgoing boundary conditions, adding an additional 150 grid points in every spatial dimension. The ECS angle is  $\theta = \pi/7 \approx 25.7^\circ$ .

Equivalent results obtained using the complex contour approach are indicated by the  $\blacktriangle$  and  $\bullet$  symbols on Figure 2. Here the Schrödinger equation (2) is first solved on a complex contour, yielding a damped solution,

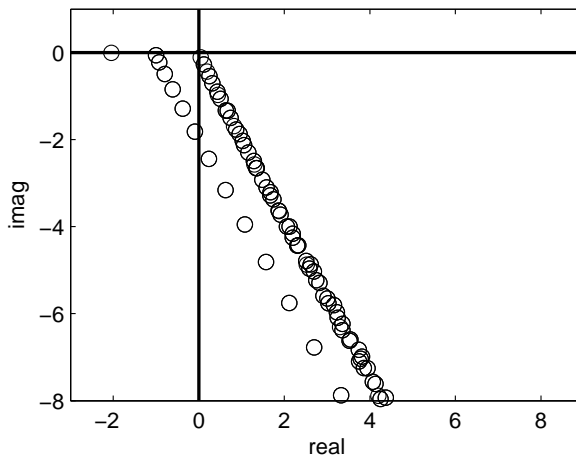


Figure 3: Spectrum (close-up) of the discretized 2D Hamiltonian (20) on a complex contour with grid distance  $he^{-i\gamma}$ , where  $h = 1/N_x = 1/N_y$  is the corresponding real-valued grid distance. The complex grid rotation angle is  $\gamma = \pi/6$ , causing the spectrum to be rotated down into the complex plane over an angle  $2\gamma = \pi/3$ .

followed by the calculation of the integrals (14) and (16) along this complex contour. For the complex contour method, a complex scaled grid with an overall complex rotation angle  $\gamma = \pi/21 \approx 8.5^\circ$  is used.

### 2.6. Spectral properties of the 2D Schrödinger operator

To obtain additional insight in the multigrid convergence, we briefly discuss the spectral properties of the discretized 2D Schrödinger operator. The discretized 2D Hamiltonian  $H^{2d}$  corresponding to equation (2) can be written as a sum of two Kronecker products and a two-body potential, i.e.

$$H^{2d} = H_1 \otimes I + I \otimes H_2 + V_{12}(x, y), \quad (20)$$

where

$$H_1 = -1/2\Delta + V_1 \quad \text{and} \quad H_2 = -1/2\Delta + V_2 \quad (21)$$

are the discretized one-dimensional Hamiltonians. When the two-body potential  $V_{12}(x, y)$  is weak relative to the one-body potentials  $V_1(x)$  and  $V_2(y)$ , the eigenvalues of the 2D Hamiltonian can be approximated by

$$\lambda^{2d} \approx \lambda_1 + \lambda_2, \quad (22)$$

where  $H_1\phi(x) = \lambda_1\phi(x)$  and  $H_2\phi(y) = \lambda_2\phi(y)$ . The spectrum of the one-dimensional Hamiltonians  $H_1$  and  $H_2$  closely resembles the spectrum of the 1D Laplacian  $(-1/2)\Delta$ ; however, the presence of the potential modifies the smallest eigenvalues, typically yielding a single (or a small number of) negative eigenvalue(s) due to the attractive potential.

The spectrum of the complex rotated 2D Schrödinger operator with  $E = 0$  is shown on Figure 3. The eigenvalues of the 2D Hamiltonian are rotated down in the complex plane when the system is discretized along a complex-valued contour. An isolated negative real eigenvalue at  $-2.043$  appears, and two series of eigenvalues emerge from the real axis at  $-1.012$  and  $0$  respectively. The leftmost branch of eigenvalues originates from the sum of the negative eigenvalue of the first 1D Hamiltonian  $H_1$  combined with all the positive eigenvalues of the second 1D Hamiltonian  $H_2$ , and vice versa. The second series of eigenvalues starting at the origin is approximately formed by the sums of the positive eigenvalues of both one-dimensional

Hamiltonians. The isolated eigenvalue and leftmost branch correspond to so-called bound states, i.e. highly oscillatory localized 1D waveforms propagating close to the  $x = 0$  and  $y = 0$  axes. Depending on the sign of the energy  $E$ , the Hamiltonian eigenvalues shown on Figure 3 are shifted to the left or right. For some negative energies  $E < 0$ , this might result in an eigenvalue located close to zero, which causes most iterative solvers (including standard multigrid) to suffer from a severe convergence slow down. This observation forms the major motivation for the development of an additional correction scheme to support the multigrid solver. The Coupled Channel Correction Scheme introduced in the next section is designed specifically to account for the bound state eigenmodes.

### 3. MG-CCCS: a multigrid-based solver which includes a Coupled Channel Correction Scheme

It was shown in [9] that multigrid generally acts as an efficient solution scheme for the discretized Schrödinger system (11) when the latter is represented along a complex contour. However, it was also observed that multigrid convergence tends to stagnate in certain energy regimes. Notably, a deterioration in convergence occurs when the problem is not fully broken up in its subparticles, in which case the convergence rate is strongly affected by the presence of bound states, cf. Section 2.6. In this section, we present a correction scheme that can be used in addition to the standard multigrid scheme, and which is designed specifically at resolving the low-dimensional single ionization waves in the solution. Using the Coupled Channel approximation we obtain a system of  $(d - 1)$ -dimensional Coupled Channel equations, which can be solved directly due to the dimension reduction, and can consequently be used to correct the solution. The separate handling and elimination of the bound states from the error results in an overall more robust iterative solution scheme. We derive the Coupled Channel scheme in a 2D problem setting for notational and implementation convenience.

#### 3.1. The Coupled Channel approximation

The aim of the correction scheme is to approximately solve the driven Schrödinger equation

$$(H - E)u(x, y) = (H_1 + H_2 + V_{12}(x, y) - E)u(x, y) = f(x, y) \quad (23)$$

for an energy  $E$  where single ionization waves dominate the solution. This implies that in large parts of the domain the solution can be written as the product of an outgoing wave in one coordinate with an eigenstate in the other coordinate. Let us assume that the 1D Hamiltonians  $H_1$  and  $H_2$  are such that there are eigenstates

$$H_1\phi_n(x) = \lambda_n\phi_n(x), \quad (24)$$

and

$$H_2\varphi_n(y) = \mu_n\varphi_n(y), \quad (25)$$

for which  $\lambda_n < 0$  and  $\mu_n < 0$  are negative. Using the so-called Coupled Channel approximation, we approximate a given function  $u(x, y)$  as

$$u(x, y) \approx \sum_{m=1}^M A_m(y)\phi_m(x) + \sum_{l=1}^L B_l(x)\varphi_l(y) \quad (26)$$

where  $M$  and  $L$  are assumed to be much smaller than the number of discretization points in each respective spatial dimension. The coefficient functions  $A_m$  and  $B_l$  represent, for example, the asymptotic form of a single ionization outgoing wave, for which it is known that  $\lim_{y \rightarrow \infty} u(x, y) = \sum_{m=1}^M S_m \exp(ik_m y)\phi_m(x)$ , where  $S_m$  are the single ionization amplitudes and  $k_m = \sqrt{2(E - \lambda_m)}$ .

**Remark.** Note that the approximate expansion (26) is generally not uniquely defined. Indeed, we can add arbitrary linear combinations of the eigenfunctions  $\varphi_l(y)$  to  $A_m(y)$  without modifying the approximation.

For example, adding  $\sum_{l=1}^L \alpha_{lm} \varphi_l(y)$  to  $A_m(y)$  is compensated by subtracting a similar linear combination of the eigenmodes  $\phi_m(x)$  from  $B_l(x)$ , i.e.

$$\begin{aligned} \sum_{m=1}^M \left( A_m(y) + \sum_{l=1}^L \alpha_{lm} \varphi_l(y) \right) \phi_m(x) + \sum_{l=1}^L \left( B_l(x) - \sum_{m=1}^M \alpha_{lm} \phi_m(x) \right) \varphi_l(y) \\ = \sum_{m=1}^M A_m(y) \phi_m(x) + \sum_{l=1}^L B_l(x) \varphi_l(y). \end{aligned}$$

To define a unique representation of the form (26), we choose, without loss of generality,  $A_m(y)$  and  $B_l(x)$  such that (for  $1 \leq i \leq M$ ,  $1 \leq j \leq L$ )

$$a_{ji} := \int_0^\infty A_i(y) \varphi_j(y) dy = 0, \quad \forall j > i, \quad (27)$$

and

$$b_{ij} := \int_0^\infty B_j(x) \phi_i(x) dx = 0, \quad \forall i \geq j. \quad (28)$$

Note, however, that any other convention, for example that all  $a_{ji} = 0$  for all  $i, j$ , would also be possible. Given a known function  $u(x, y)$  we can now calculate the corresponding coefficient functions  $A_m(y)$  and  $B_l(x)$  of the Coupled Channel approximation as follows. For  $1 \leq i \leq M$  it holds that

$$A_i(y) = \int_0^\infty u(x, y) \phi_i(x) dx - \sum_{l=1}^L \left( \int_0^\infty B_l(x) \phi_i(x) dx \right) \varphi_l(y) = \int_0^\infty u(x, y) \phi_i(x) dx - \sum_{l=1}^L b_{il} \varphi_l(y), \quad (29)$$

and for  $1 \leq j \leq L$  we have

$$B_j(x) = \int_0^\infty u(x, y) \varphi_j(y) dy - \sum_{m=1}^M \left( \int_0^\infty A_m(y) \varphi_j(y) dy \right) \phi_m(x) = \int_0^\infty u(x, y) \varphi_j(y) dy - \sum_{m=1}^M a_{jm} \phi_m(x). \quad (30)$$

Hence, the coefficients  $a_{ji}$  and  $b_{ij}$  need to be computed in order to calculate  $A_i(y)$  and  $B_j(x)$ . These coefficients can be calculated directly from the function  $u(x, y)$  by integration, since it holds that

$$\int_0^\infty \int_0^\infty \phi_i(x) \varphi_j(y) u(x, y) dx dy = a_{ji} + b_{ij}. \quad (31)$$

Since  $b_{ij}$  is zero while  $a_{ji}$  is non-zero and vice versa due the uniqueness conventions (27)-(28), the coefficients  $a_{ji}$  and  $b_{ij}$  are indeed uniquely defined by (31), and hence the expansion (26) can be computed.

### 3.2. The Coupled Channel projection space

Given the 2D driven Schrödinger equation, we now represent both the unknown solution and the known right-hand side in a factorized way using the Coupled Channel approximation (26). Equation (23) then becomes

$$(H_1 + H_2 + V_{12}(x, y) - E) \left( \sum_{m=1}^M A_m(y) \phi_m(x) + \sum_{l=1}^L B_l(x) \varphi_l(y) \right) = \sum_{m=1}^M f_m^A(y) \phi_m(x) + \sum_{l=1}^L f_l^B(x) \varphi_l(y), \quad (32)$$

where  $f_m^A$  and  $f_l^B$  are uniquely defined, cf. (27)-(28), and can be calculated explicitly. A decomposition of this equation gives rise to a pair of coupled systems of equations. The first system reads

$$(H_1 + H_2 + V_{12}(x, y) - E) \left( \sum_{m=1}^M A_m(y) \phi_m(x) \right) = \sum_{m=1}^M f_m^A(y) \phi_m(x). \quad (33)$$

Using the fact that  $H_1\phi_n(x) = \lambda_n\phi_n(x)$ , multiplying the above equation with  $\phi_i(x)$  (for  $1 \leq i \leq M$ ) and integrating over  $x$  yields

$$(H_2 + \lambda_i - E) A_i(y) + \sum_{m=1}^M \left( \int_0^\infty V_{12}(x, y) \phi_i(x) \phi_m(x) dx \right) A_m(y) = f_i^A(y). \quad (34)$$

Note that we use a specific normalization of the eigenmodes in order to obtain the above equation.<sup>1</sup> Introducing the notation  $V_{im}^A(y) := \int_0^\infty V_{12}(x, y) \phi_i(x) \phi_m(x) dx$  ( $1 \leq i, m \leq M$ ), this ultimately results in the Coupled Channel equation for  $A_i(y)$

$$(H_2 + \lambda_i + V_{ii}^A(y) - E) A_i(y) + \sum_{\substack{m=1 \\ m \neq i}}^M V_{im}^A(y) A_m(y) = f_i^A(y) \quad \text{for } i = 1, \dots, M. \quad (35)$$

In a similar way, one can derive a coupled system for  $B_j(x)$

$$(H_1 + \mu_j + V_{jj}^B(x) - E) B_j(x) + \sum_{\substack{l=1 \\ l \neq j}}^L V_{jl}^B(y) B_l(x) = f_j^B(y) \quad \text{for } j = 1, \dots, L, \quad (36)$$

where  $V_{jl}^B(y) := \int_0^\infty V_{12}(x, y) \varphi_j(y) \varphi_l(y) dy$  ( $1 \leq j, l \leq L$ ). These equations are known as the Coupled Channel equations and are frequently used to describe electronic states in atoms and molecules, see [15].

For the 2D Schrödinger system (23) the corresponding Coupled Channel equations (35)-(36) form a set of  $M+L$  one-dimensional equations that need to be solved in order to obtain the Coupled Channel representation (26) for the solution  $u(x, y)$ . Hence, the Coupled Channel approximation can be considered as a dimension reducing projection of the 2D solution  $u(x, y)$  unto a collection of 1D subproblems.

### 3.3. The Coupled Channel Correction Scheme

We now use the Coupled Channel equations (35)-(36) to define a correction scheme for the solution of the driven Schrödinger equation. Let  $u^{(k)}(x, y)$  be a  $k$ -th guess for the solution of equation (23), which was computed by some iterative solution scheme (e.g. a series of multigrid V-cycles). An improved guess  $u^{(k+1)}$  can be obtained with the help of the following correction scheme. We first formulate the error equation

$$(H - E) e^{(k)}(x, y) = r^{(k)}(x, y), \quad (37)$$

where  $e^{(k)}(x, y) = u(x, y) - u^{(k)}(x, y)$  is the current guess error and  $r^{(k)} = f(x, y) - (H - E) u^{(k)}(x, y)$  is the corresponding residual. Instead of solving the error equation exactly, which is as hard as solving the original problem, we solve it approximately using the Coupled Channel approximation (26). We expand the residual and error functions using the Coupled Channel approximation, such that

$$r^{(k)}(x, y) = \sum_{m=1}^M r_m^A(y) \phi_m(x) + \sum_{l=1}^L r_l^B(x) \varphi_l(y), \quad (38)$$

and

$$e^{(k)}(x, y) = \sum_{m=1}^M e_m^A(y) \phi_m(x) + \sum_{l=1}^L e_l^B(x) \varphi_l(y). \quad (39)$$

---

<sup>1</sup>Throughout this work we use an alternative normalization of the complex-valued eigenmodes  $\phi$  given by  $\int_0^\infty \phi(z)^2 dz = 1$ , rather than the more commonly used Hermitian inner product with complex conjugation. In this way the complex-valued eigenmodes are normalized identically to the normalization on the real-valued domain where the Hamiltonian is Hermitian.

Here the coefficient functions  $r_m^A(y)$  and  $r_l^B(x)$  for the residual are known. Subsequently, the Coupled Channel equations are solved for the error coefficient functions  $e_i^A(y)$  and  $e_j^B(x)$ :

$$(H_2 + \lambda_i + V_{ii}^A(Y) - E) e_i^A(y) + \sum_{\substack{m=1 \\ m \neq i}}^M V_{im}(y) e_m^A(y) = r_i^A(y) \quad \text{for } i = 1, \dots, M, \quad (40)$$

$$(H_1 + \mu_j + V_{jj}^B(x) - E) e_j^B(x) + \sum_{\substack{l=1 \\ l \neq j}}^L V_{jl}^B(y) e_l^B(x) = r_j^B(y) \quad \text{for } j = 1, \dots, L. \quad (41)$$

The solution of these one-dimensional systems is significantly easier than solving the original 2D driven Schrödinger system (23). Indeed, the reduction in spatial dimension allows us to effectively solve the Coupled Channel systems using a direct solution method, which yields a fast and accurate solution. We then correct the current guess for the solution by adding the Coupled Channel approximation of the error to the current solution  $u^{(k)}(x, y)$  in the Coupled Channel correction step

$$u^{(k+1)}(x, y) = u^{(k)}(x, y) + \sum_{m=1}^M e_m^A(y) \phi_m(x) + \sum_{l=1}^L e_l^B(x) \varphi_l(y). \quad (42)$$

We remark that the extension of the above Coupled Channel Correction Scheme to higher spatial dimensions, notably 3D, can theoretically be obtained in an analogous manner. This 3D correction scheme would be based upon a double Coupled Channel approximation, introducing a correction in function of both the 1D and 2D eigenstates to account for the presence of one- and two-dimensional bound states travelling along the axes and faces of the coordinate system respectively. This leads to both 1D and 2D pairs of coupled systems of equations, which are in turn significantly easier to solve than the full 3D break-up problem. Although we believe the generalization to higher dimensions is straightforward, we do not expound on the 3D Coupled Channel Correction Scheme in this work for notational and implementation ease. Instead, we aim to tackle this problem in future work.

#### 4. Implementation and numerical accuracy

Additional care is required for the calculation of the eigenstates involved in the scattering process when the coordinates are rotated into the complex plane. For photoionization problems, the right-hand side is typically the dipole operator applied to the eigenstate with the lowest energy [28]. However, for impact ionization problems the right-hand side contains the incoming wave that consists of a target state, i.e. the eigenstate with the lowest energy, and a purely incoming wave representing the incoming particle [1, 18]. Both of these functions require a careful and accurate numerical description, especially on the complex contour, since after complex rotation the incoming wave becomes an exponentially increasing function.

##### 4.1. The complex contour rotation angle and numerical accuracy

In this section we comment on some key numerical aspects of the proposed complex contour approach. Note that from a theoretical point of view the real-valued integral (13) and its counterpart evaluated along the complex contour (19) are identical, independently of the size of the rotation angle  $\gamma$ . Indeed, in principle the rotation angle can be chosen arbitrarily large, implying very strong damping, which is beneficial for the multigrid solver. However, in reality a restriction on the size of the rotation angle is imposed by the numerical implementation. We illustrate this claim on a 2D Temkin-Poet model problem, where it is shown that when the angle of rotation is too large and the potential is long range, significant numerical inaccuracies occur.

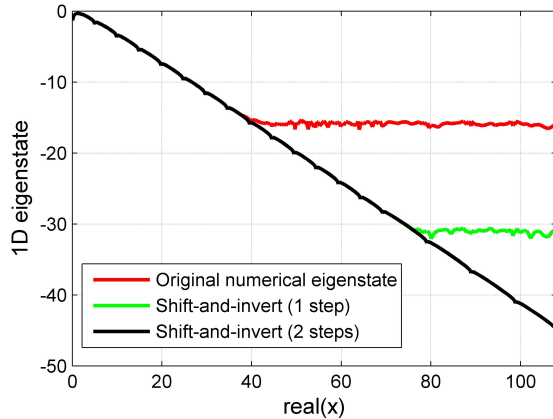


Figure 4: Modulus of the 1D eigenstate  $\phi_n(x)$  calculated numerically along the complex contour with  $\gamma = 9^\circ$ . Plot in function of the real part of the complex-valued  $x$ -coordinate. Shown is the numerical eigenstate calculated ‘naïvely’ using a standard eigenfunction routine (red) and the eigenstate with improved accuracy using several steps of shift-and-invert (green and black). Round-off errors are eliminated after two applications of the shift-and-invert technique. Vertical axis in log-scale.

#### 4.1.1. The 2D Temkin-Poet model: propagation of round-off errors in the eigenstates

We consider the 2D Temkin-Poet model discretized using a spectral element type discretization; however, the following observations are independent of the exact discretization scheme. The total wave  $u(x, y)$  is the sum of the incoming wave  $u_{in}$  and the scattered wave  $u_{sc}$ , i.e.

$$u(x, y) = u_{in}(x, y) + u_{sc}(x, y). \quad (43)$$

Hence, the far field integral (19) can be effectively split up into a sum of two integrals: one over  $u_{in}$  and the other over  $u_{sc}$ . The latter integral is easy to evaluate, since the scattered wave solution  $u_{sc}$  is exponentially decaying on the complex contour. The integral over  $u_{in}$  is more challenging from a numerical perspective, since for the impact ionization model we have

$$u_{in}(x, y) = \phi_n(x) \sin(k_n y), \quad (44)$$

with  $k_n = \sqrt{2(E - \lambda_n)}$ , where  $\phi_n$  is an eigenstate of the one-body operator (8) with a negative eigenvalue  $\lambda_n$ . On the real-valued domain the eigenstate  $\phi_n$  is an exponentially decaying function, since  $\lambda_n < 0$  implies that  $\phi_n$  asymptotically behaves as  $\exp(\lambda_n x)$ . After complex coordinate rotation  $\phi_n$  is still a decaying function, yet it is now slightly oscillating because of the acquisition of the imaginary part by  $x$ . However, when calculated numerically using a standard eigenfunction routine, the exponential decay of  $\phi_n$  is unavoidably truncated at machine precision. This is illustrated in Figure 4, where it is observed that from a certain distance on the exponential decay stagnates.

Subsequently, to form the incoming wave, the eigenstate is multiplied by  $\sin(k_n y)$ . However, on the complex rotated grid the latter becomes an exponentially growing function in  $y$ , with the exponential growth being governed by the rotation angle  $\gamma$ . The truncated part of the eigenstate  $\phi_n$  that should be negligibly small hence becomes substantial for larger values of  $y$  through the multiplication. Hence, the numerical round-off of the 1D eigenstate  $\phi_n$  produces a large and unwanted error which propagates through the algorithm. The incoming wave  $u_{in}$  is consequently multiplied by the potential  $V_{12}$  and subtracted from the right-hand side  $f$  to form the far field integrand, cf. (19). The resulting function is heavily contaminated due to the numerical round-off errors in  $\phi_n$ , as is shown in the left panel of Figure 5. The contaminations at the outgoing edges of the domain ( $x, y \rightarrow \infty$ ) are due to the numerical round-off phenomenon described above.

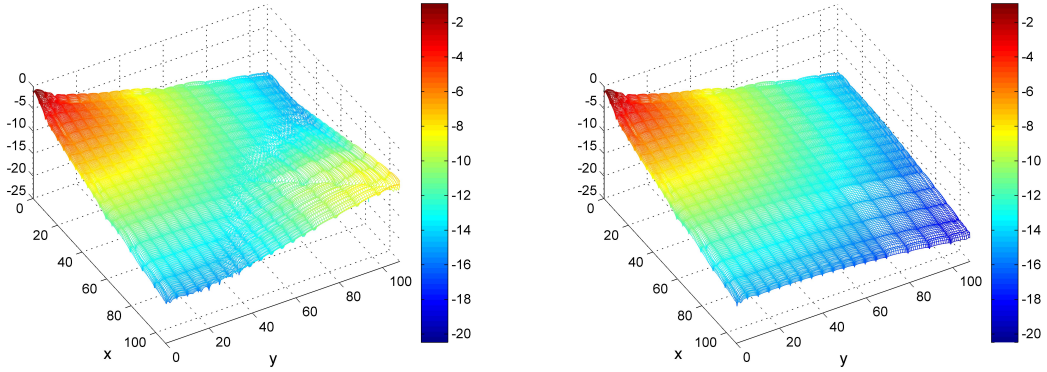


Figure 5: Modulus of the function  $f(x, y) - V_{12}(x, y)\phi_n(x)\sin(k_n y)$ , part of the integrand in (19), calculated numerically on the complex contour with  $\gamma = 9^\circ$  for energy  $E = 1$ . Plot in function of the real part of the complex-valued  $x$ - and  $y$ -coordinates. Vertical axis in log-scale. Left: with standard eigenfunction computation of  $\phi_n(x)$  (naïve calculation). Round-off errors contaminate the function for  $x, y \rightarrow \infty$ , cf. Figure 4. Right: adapted computation using the iteratively refined eigenstate  $\phi_n(x)$ ; round-off errors have been eliminated.

#### 4.1.2. Solution to the truncation errors: shift-and-invert

To account for the numerical inaccuracies due to the round-off of the 1D eigenstates, we apply the classical concept of shift-and-invert [16] to the eigenstate  $\phi_n$ , which is closely related to iterative refinement [29]. This simple iterative update step (power iteration) is based on an additional solve using the shifted Hamiltonians  $(H_1 - \lambda_n)$  or  $(H_2 - \lambda_n)$ , hence allowing for a more accurate representation of the exponentially decaying eigenstates  $\phi_n$ . The resulting numerical eigenstate after application of the shift-and-invert technique is shown on Figure 4. Using an improved representation of the eigenstates, the round-off errors due to multiplication by the exponentially increasing sine function can be avoided, as illustrated in the right panel of Figure 5.

Note that the complex rotation angle  $\gamma$  plays an important role in the numerical accuracy and the avoiding of round-off errors. Even when improving the numerical accuracy of the eigenstates  $\phi_n(x)$  and  $\varphi_n(y)$  using the shift-and-invert technique as suggested above, the multiplication by  $\sin(k_n y)$  and  $\sin(k_n x)$  respectively should be treated with care. Indeed, if  $\gamma$  is chosen too large, the exponential growth of the sine functions may still introduce a blow-up of round-off errors in the computation. To avoid this issue, the rotation angle  $\gamma$  should, as a general rule of thumb, always be chosen as small as possible, under the condition that the multigrid scheme be stable. This trade-off in the choice of the complex rotation is characteristic for complex shifted/rotated problems, cf. [13, 10].

#### 4.2. Validation of the complex contour approach: computation of the ionization cross sections

Following the discussion in the previous section, the cross section  $\zeta(k_1, k_2)$  of the 2D Temkin-Poet model problem can now be calculated accurately. The TP model problem features potentials  $V_1(x) = -1/x$ ,  $V_2(y) = -1/y$  and  $V_{12}(x, y) = 1/\max(x, y)$ , and the right-hand side is given by  $f(x, y) = xy \exp(-(x + y)^2)$ . The double ionization cross section is given by expression (16), where  $k_1 = \sqrt{2E} \sin(\alpha)$  and  $k_2 = \sqrt{2E} \cos(\alpha)$ . Hence, the cross section  $\zeta(k_1, k_2)$  can be calculated for a single energy  $E$  in function of the incoming wave angle  $\alpha \in [0, \pi/2]$  to yield the single differential cross section (SDCS). The total cross section (TCS)  $\sigma_{tot}(E)$  can then be calculated as an integral of  $\zeta$  over all energies up to a certain value of  $E$ , and is given by expression (17) in function of the energy of the system.

Figure 6 (left panel) shows the single differential cross section for the 2D Temkin-Poet model problem for the energy  $E = 1$ , at which a full break-up of the system (double ionization) occurs. The scattering solution

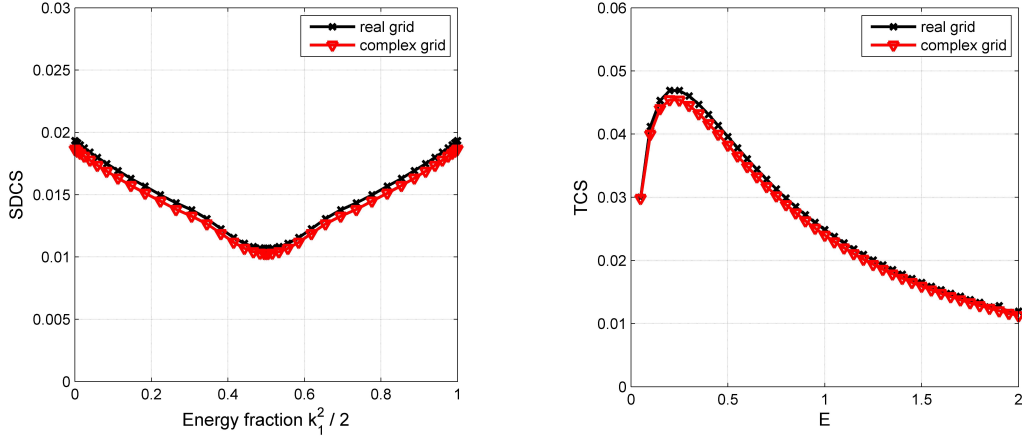


Figure 6: Left: Single differential cross section  $\zeta(k_1, k_2)$  (16) in function of the energy fraction  $k_1^2/2 \in [0, 1]$ . Right: Total double ionization cross section  $\sigma_{tot}(E)$  (17) in function of the energy  $E \in [0, 2]$ . Black: classical calculation on the real-valued domain using ECS boundaries with  $\theta_{ECS} = 30^\circ$ . Red: alternative calculation on the complex-valued domain with  $\gamma = 9^\circ$ .

is computed using a spectral element discretization of the domain  $\Omega = [0, 108]^2$  using  $N_x = N_y = 269$  grid points in every spatial direction. The SDCS is computed on both the complex contour domain with  $\gamma = 9^\circ$  and the classical real-valued domain with an ECS absorbing boundary layer ( $\theta_{ECS} = 30^\circ$ ) for comparison. Note that to avoid propagation of numerical eigenstate round-off errors throughout the algorithm, the shift-and-invert technique is applied to the 1D eigenmodes to ensure numerical accuracy. The complex contour approach yields an accurate representation of the SDCS compared to the computation using the classical real-valued method.

The total cross section for the 2D Temkin-Poet model problem is shown in Figure 6 (right panel) for a range of energies  $E \in [0, 2]$  for which both single and double ionization occur simultaneously. The figure validates the complex contour approach by comparing the TCS computed using the classical real-valued domain to the computation of the cross section using the complex contour approach, where notably 2 steps of shift-and-invert are included for numerical accuracy. The resulting total cross section is close to identical for both methods.

## 5. Numerical results: convergence of the MG-CCCS method

In this section we validate the efficiency and scalability of the Multigrid-Coupled Channel (MG-CCCS) combined method in solving the damped Schrödinger equation along a complex contour. We illustrate the convergence of the MG-CCCS method both as a solver and a Krylov preconditioner. When used as a Krylov preconditioner, only one MG-CCCS V-cycle is used to approximately solve the preconditioning system, as is common practice in the multigrid literature [13, 4]. We present convergence results for two distinct model problems: a 2D ionization problem with exponentially decaying potentials, and a 2D Temkin-Poet benchmark problem.

### 5.1. The 2D ionization model with exponential potentials

As a proof of concept, we first consider a simple 2D electron-impact ionization model problem with exponentially decreasing potentials. The potentials are given by  $V_1(x) = -4.5 \exp(-x^2)$ ,  $V_2(y) = -4.5 \exp(-y^2)$  and  $V_{12}(x, y) = 2 \exp(-0.1(x+y)^2)$ . The right-hand side is  $f(x, y) = \exp(-3(x+y)^2)$ . The corresponding driven Schrödinger equation (2) is solved along a complex contour with rotation angle  $\gamma = \pi/18 = 10^\circ$  on a uniform discretization of the domain  $\Omega = [0, 20]^2$  featuring  $N_x = N_y = 256$  grid points in every spatial direction. This

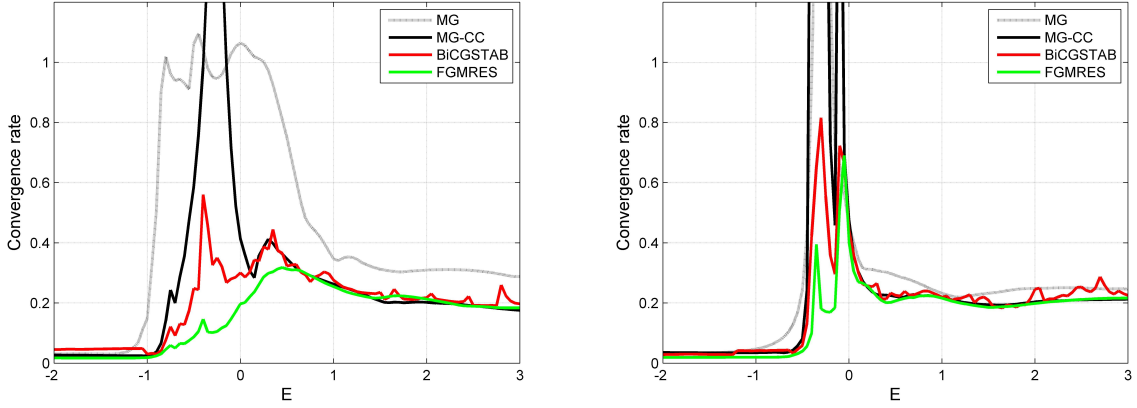


Figure 7: Comparison of the convergence rates of different iterative solution methods for two 2D complex contour Schrödinger model problems. Classical MG is used as a solver only. The MG-CCCS method (with  $M = L = 2$ ) is used both as a stand-alone solver and Krylov preconditioner for BiCGSTAB and FGMRES. Left: exponential potentials model problem, domain  $[0, 20]^2$ , no. grid points  $N_x = N_y = 256$ , no. MG levels  $l = 8$ . Right: Temkin-Poet model problem, domain  $[0, 100]^2$ , no. grid points  $N_x = N_y = 1024$ , no. MG levels  $l = 10$ .

discretization implies a minimum of 20 grid points per wavelength is guaranteed for all energies  $E \in [-2, 3]$ , yielding an accurate representation of the waveforms.

Figure 7 (left panel) compares the convergence rate of the classical multigrid method to the MG-CCCS, MG-CCCS BiCGSTAB and MG-CCCS FGMRES solvers in function of the energy  $E$ . The MG scheme denotes the standard multigrid method using V(1,1)-cycles with a GMRES(3) pre- and post-smoothing substitute. The MG-CCCS scheme includes a Coupled Channel correction step with  $L = M = 2$  after each V-cycle. The classical MG solver is unstable in the region of energies for which only single ionization occurs, i.e. for  $E \in [-1, 0]$ , cf. conclusions drawn in [9]. In principle the energy regimes for which only single ionization occurs do not require a full 2D description, since a 1D model would suffice to describe the single ionization waveforms. However, rather than adapting the mathematical model description to the energy  $E$ , we in this work aim at constructing a robust 2D solver that is effective for *all* energy regimes. The MG-CCCS solver features improved convergence for most energy levels due to the additional elimination of 1D evanescent modes from the error. This implies the overall convergence of the MG-CCCS scheme is significantly better than the standard MG convergence rate. Stability of the MG-CCCS scheme is unfortunately still not guaranteed for every energy. The MG-CCCS scheme can be used as a preconditioner to a general Krylov method to further improve stability. Acceleration of the MG-CCCS scheme by a governing Krylov solver leads to a solution method which is guaranteed to be stable over the entire energy regime. The MG-CCCS preconditioned BiCGSTAB solver features a convergence rate of less than 0.6 for all energy regimes, while the restarted FGMRES(5) features a convergence rate of at most 0.32 for all energies. The MG-CCCS Krylov solver hence proves to be a robust solution method for the 2D ionization model problem.

## 5.2. The 2D Temkin-Poet model

We now consider a more realistic Temkin-Poet benchmark problem on a large domain  $\Omega = [0, 100]$ , requiring a fine discretization of  $N_x = N_y = 1024$  grid points to satisfy the wavenumber criterion of 20 points per wavelength for all energies  $E \in [-2, 3]$ . The Temkin-Poet potentials are  $V_1(x) = -1/x$ ,  $V_2(y) = -1/y$  and  $V_{12}(x, y) = 1/\max(x, y)$ , and the right-hand side for this problem is again  $f(x, y) = \exp(-3(x + y)^2)$ .

The convergence rates for the 2D Temkin-Poet model are shown in the right panel of Figure 7. Note how the effect of the Coupled Channel correction is somewhat less pronounced for the TP model problem. Indeed,

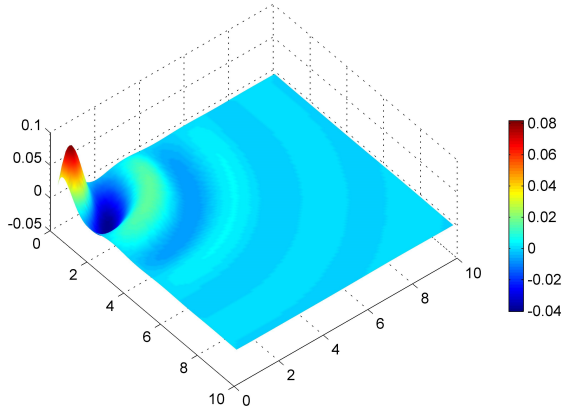


Figure 8: Numerical solution  $u^N$  to the 2D complex-valued Temkin-Poet model problem with energy  $E = 1$ . Discretization of the domain  $\Omega = [0, 200]^2$  using a total of  $2048^2$  grid points. Displayed is a close-up of the solution on the subdomain  $[0, 10]^2$ . The exponential decay of the solution on the complex rotated grid is clearly visible. Solution method details: see Table 1.

	domain $\Omega$ $N_x \times N_y$	$[0, 10]^2$ $128^2$	$[0, 20]^2$ $256^2$	$[0, 50]^2$ $512^2$	$[0, 100]^2$ $1024^2$	$[0, 200]^2$ $2048^2$
$E = 1$	iterations	6	7	7	7	7
	CPU time	0.5 s.	2.1 s.	9.0 s.	36.9 s.	145.1 s.
$E = 2$	iterations	7	7	7	7	7
	CPU time	0.6 s.	2.0 s.	9.0 s.	35.4 s.	140.4 s.
$E = 3$	iterations	7	7	8	8	8
	CPU time	0.6 s.	2.0 s.	10.3 s.	40.1 s.	162.0 s.

Table 1: Scalability results for the 2D complex-valued Temkin-Poet model problem with energies  $E = 1, 2, 3$  in the full double ionization regime. MG-CCCS preconditioned FGMRES ( $M = L = 2$ ) iteration count and CPU time required to solve the problem up to a relative residual tolerance of  $10^{-6}$  in function of problem size. Discretizations respecting the 20 points per wavelength criterion.

a lesser improvement in convergence rate is measured when comparing the classical MG and MG-CCCS schemes. However, the MG-CCCS preconditioned Krylov solvers again provide a stable solution method for all energies. Convergence rates for the MG-CCCS FGMRES solver generally lie below 0.30, with the exception of a small outlier at slightly negative energies where it rises to around 0.70. Convergence of the MG-CCCS Krylov solver is guaranteed for all  $E \in [-2, 3]$ , yielding a robust solver for all energy regimes.

Table 1 shows the scalability of the MG-CCCS preconditioned FGMRES solver for the Temkin-Poet model problem for different fixed energy levels  $E = 1, 2$  and  $3$ . Note that these energies represent regions of physical interest where single and double ionization simultaneously occur. The number of MG-CCCS FGMRES iterations and CPU time<sup>2</sup> required to solve the problem up to a relative residual tolerance of  $10^{-6}$  are displayed in function of the number of grid points (increasingly more accurate discretization). Quasi perfect  $\mathcal{O}(N)$  scalability can be observed from the table. The number of Krylov iterations remains constant as the number of discretization points increases, resulting in a CPU time which effectively scales linearly in the number of unknowns. Moreover, good scalability in function of the energy level is guaranteed. Hence, the MG-CCCS preconditioned Krylov method is not only robust to different energies as shown by Figure 7, it additionally exhibits optimal scaling properties.

<sup>2</sup>System specifications: Intel Core i7-2720QM 2.20GHz CPU, 6MB Cache, 8GB RAM.

## 6. Conclusions

In this paper we have developed a significantly improved multigrid-based computational scheme for the calculation of the ionization cross sections of a Schrödinger-type quantum mechanical break-up problem. The method is based on the so-called complex contour approach [9], i.e. a reformulation of the classical real-valued far field integral (cross section) to an integral over a complex rotated domain. The numerical solution to the underlying driven Schrödinger system (scattered wave) on the complex-valued domain is much easier to obtain iteratively, which overcomes the primary computational bottleneck for the calculation of the ionization cross sections.

The MG-CCCS method proposed in this work combines the functionality of multigrid on the complex-rotated (damped) Schrödinger problem with a Coupled Channel Correction Scheme, which accounts for the existence of bound states in the solution that might deteriorate the multigrid convergence. Potentially accelerated by a Krylov subspace method for improved stability, the MG-CCCS solver is capable of efficient computation of the complex-valued scattered wave for any energy  $E$ , featuring optimal  $\mathcal{O}(N)$  scalability in the number of unknowns. Furthermore, the Coupled Channel Correction Scheme improves the stability of the classical multigrid method, ensuring robustness of the MG-CCCS Krylov solver relative to the energy of the system.

Particular care is advised when representing the impact ionization problem on the complex-valued domain, since the complex integral implementation is prone to round-off errors due to the exponential decay and growth of the eigenstates and incoming wave components respectively. Consequently, numerical round-off errors might propagate through the algorithm and contaminate the resulting cross sections if not treated properly. We suggest the use of shift-and-invert to ensure proper accuracy of the eigenstate functions. The choice of the complex rotation angle is of fundamental importance in this regard, since it governs the rate of exponential growth of certain integrand components. Hence, the rotation angle is bounded both from below by the requirement of a stable multigrid solver, and from above by the numerical accuracy of the implementation. A trade-off between these two conditions should be achieved in order to obtain a functional computational scheme.

Numerical results on the 2D Temkin-Poet benchmark problem validate the proposed MG-CCCS complex contour approach, showing the method to yield an accurate representation of the single differential and total double ionization cross sections for the two-body electron break-up problem. Although the results provided in this paper are restricted to 2D model problems for notational and implementation convenience, the extension of the proposed MG-CCCS method to higher spatial dimensions, notably the three-particle break-up system, is straightforward and will be treated as part of future work.

As a final remark, we note that the Coupled Channel Correction Scheme proposed in this work was implemented as an explicit additional step to increase the performance of the multigrid preconditioner. However, it could alternatively be embedded in the governing Krylov solver in the form of a deflation step, cf. the work by Sheikh et al. in [24], which analogously aims at eliminating problematic eigenstates in the solution, and may in this regard lead to an even more efficient solver.

## 7. Acknowledgments

This research is funded by the Research Council of the University of Antwerp. The authors additionally thank Bram Reps for fruitful discussions on the subject.

## References

- [1] M. Baertschy, T.N. Rescigno, W.A. Isaacs, X. Li, and C.W. McCurdy. Electron-impact ionization of atomic hydrogen. *Physical Review A*, 63(2):022712, 2001.

- [2] E. Balslev and J.M. Combes. Spectral properties of many-body Schrödinger operators with dilatation-analytic interactions. *Communications in Mathematical Physics*, 22(4):280–294, 1971.
- [3] J.-P. Berenger. A perfectly matched layer for the absorption of electromagnetic waves. *Journal of computational physics*, 114(2):185–200, 1994.
- [4] M. Bollhöfer, M.J. Grote, and O. Schenk. Algebraic multilevel preconditioner for the Helmholtz equation in heterogeneous media. *SIAM Journal on Scientific Computing*, 31(5):3781–3805, 2009.
- [5] A. Brandt. Multi-level adaptive solutions to boundary-value problems. *Mathematics of computation*, 31(138):333–390, 1977.
- [6] W.L. Briggs, V.E. Henson, and S.F. McCormick. *A Multigrid Tutorial*. Society for Industrial Mathematics, Philadelphia, 2000.
- [7] H. Calandra, S. Gratton, R. Lago, X. Pinel, and X. Vasseur. Two-level preconditioned Krylov subspace methods for the solution of three-dimensional heterogeneous Helmholtz problems in seismics. Technical report, TR/PA/11/80, CERFACS, Toulouse, France, 2011.3, 2011.
- [8] D.L. Colton and R. Kress. *Inverse acoustic and electromagnetic scattering theory*, volume 93. Applied Mathematical Sciences, Springer, 1998.
- [9] S. Cools, B. Reps, and W. Vanroose. An efficient multigrid calculation of the far field map for Helmholtz and Schrödinger equations. *SIAM Journal on Scientific Computing*, 36(3):B367–B395, 2014.
- [10] S. Cools and W. Vanroose. Local Fourier analysis of the complex shifted Laplacian preconditioner for Helmholtz problems. *Numerical Linear Algebra with Applications*, 20(4):575–597, 2013.
- [11] H. Elman, M. Mihajlović, and D. Silvester. Fast iterative solvers for buoyancy driven flow problems. *Journal of Computational Physics*, 230(10):3900–3914, 2011.
- [12] H.C. Elman, O.G. Ernst, and D.P. O’Leary. A multigrid method enhanced by Krylov subspace iteration for discrete Helmholtz equations. *SIAM Journal on Scientific Computing*, 23(4):1291–1315, 2002.
- [13] Y.A. Erlangga, C.W. Oosterlee, and C. Vuik. A novel multigrid based preconditioner for heterogeneous Helmholtz problems. *SIAM Journal on Scientific Computing*, 27(4):1471–1492, 2006.
- [14] O.G. Ernst and M.J. Gander. Why it is difficult to solve Helmholtz problems with classical iterative methods. In *Numerical Analysis of Multiscale Problems. Durham LMS Symposium*. Citeseer, 2010.
- [15] H. Friedrich. *Theoretical atomic physics*, volume 3. Springer, 2006.
- [16] R.G. Grimes, J.G. Lewis, and H.D. Simon. A shifted block Lanczos algorithm for solving sparse symmetric generalized eigenproblems. *SIAM Journal on Matrix Analysis and Applications*, 15(1):228–272, 1994.
- [17] A. Kirsch. *An introduction to the mathematical theory of inverse problems*, volume 120. Applied Mathematical Sciences, Springer, 1996.
- [18] C.W. McCurdy, M. Baertschy, and T.N. Rescigno. Solving the three-body Coulomb breakup problem using exterior complex scaling. *Journal of Physics B: Atomic, Molecular and Optical Physics*, 37(17):R137, 2004.
- [19] C.W. McCurdy, T.N. Rescigno, and D. Byrum. Approach to electron-impact ionization that avoids the three-body Coulomb asymptotic form. *Physical Review A*, 56(3):1958, 1997.
- [20] N. Moiseyev. Quantum theory of resonances: calculating energies, widths and cross-sections by complex scaling. *Physics Reports*, 302(5):212–293, 1998.
- [21] B. Reps, W. Vanroose, and H. bin Zubair. On the indefinite Helmholtz equation: Complex stretched absorbing boundary layers, iterative analysis, and preconditioning. *Journal of Computational Physics*, 229(22):8384–8405, 2010.
- [22] T.N. Rescigno, M. Baertschy, W.A. Isaacs, and C.W. McCurdy. Collisional breakup in a quantum system of three charged particles. *Science*, 286(5449):2474–2479, 1999.
- [23] C.D. Riyanti, Y.A. Erlangga, R.E. Plessix, W.A. Mulder, C. Vuik, and C. Oosterlee. A new iterative solver for the time-harmonic wave equation. *Geophysics*, 71(5):E57–E63, 2006.
- [24] AH Sheikh, D Lahaye, and C Vuik. On the convergence of shifted laplace preconditioner combined with multilevel deflation. *Numerical Linear Algebra with Applications*, 20(4):645–662, 2013.
- [25] B. Simon. The definition of molecular resonance curves by the method of Exterior Complex Scaling. *Physics Letters A*, 71(2):211–214, 1979.
- [26] U. Trottenberg, C.W. Oosterlee, and A. Schüller. *Multigrid*. Academic Press, New York, 2001.
- [27] H.A. Van der Vorst. *Iterative Krylov methods for large linear systems*, volume 13. Cambridge University Press, 2003.
- [28] W. Vanroose, D.A. Horner, F. Martin, T.N. Rescigno, and C.W. McCurdy. Double photoionization of aligned molecular hydrogen. *Physical Review A*, 74(5):052702, 2006.
- [29] J.H. Wilkinson. *Rounding errors in algebraic processes*. Courier Dover Publications, 1994.